Mechanisms of Amine-Catalyzed Organosilicate Hydrolysis at Circum-Neutral pH

Katya M. Delak*[,†,‡] and Nita Sahai[†,§]

Department of Chemistry, 1101 University Avenue, University of Wisconsin, Madison, Wisconsin 53706, and Department of Geology & Geophysics, 1215 West Dayton Street, University of Wisconsin, Madison, Wisconsin 53706

Received: April 3, 2006; In Final Form: June 22, 2006

Mono- and polyamines can catalyze the hydrolysis and condensation of organosilicate starting materials in biomimetic silica synthesis pathways at circum-neutral pHs and room temperature. Our study is focused on understanding the mechanistic role of amines in catalyzing the hydrolysis process that precedes condensation. We have conducted ^{29}Si NMR experimental studies over a range of temperature and pHs for the hydrolysis rates of trimethylethoxysilane (TMES), a model compound with only one hydrolyzable bond, combined with quantum mechanical hybrid density functional theory calculations of putative intermediate and transition-state structures for TMES and tetramethyl orthosilicate (TMOS). Comparison of calculated energies with experimentally determined activation energies indicates that amine catalysis of TMES is primarily a consequence of the amine's acidity at neutral pH. The proton released by the amine is transferred to the organosilicate, producing a protonated ethoxy leaving group that can be displaced by water in an S_N2 reaction. For TMOS, the activation energy of proton-transfer coupled with S_N2 substitution is comparable to that for Corriu's nucleophile-activated nucleophilic displacement, such that the mechanism of amine-catalyzed hydrolysis is dependent mostly on the ambient pH conditions as well as the type of amine. The relevance of our results to biological silica precipitation is discussed.

Introduction

Current sol−gel routes for synthesis of mesoporous silicates, such as MCM-41, utilize organosilicate precursors, involve templating by self-assembled amphiphilic molecules, and require one or more steps at extreme pH values and high temperatures.[1−4] The kinetics of organosilicate hydrolysis by strong acids and bases and the morphological effects of hydrolysis and condensation rates on the silicas produced have been investigated thoroughly by ^{29}Si NMR[5−16] and Raman/FTIR vibrational spectroscopy.[17−19] On the basis of these studies, chemical mechanisms for the reactions have been proposed that have been addressed further by ab initio computational methods.[4,20−25] There is very little information in the literature, however, on organosilicate hydrolysis mechanisms at circum-neutral pHs. This gap is now being addressed by numerous investigations into biomimetic silica formation as catalyzed by nucleophiles such as amines, alcohols, and thiols, [26−36] inspired by the observation that organisms such as diatoms and sponges, capable of producing mesoporous silica at circum-neutral pH and room temperature, contain silica-precipitating proteins where nucleophilic functional groups such as amines and alcohols are central to the catalytic function of the protein.[37−40]

The biomimetic approach is based on using molecules that mimic protein activity and complements potential, new, genomic approaches where mesoporous silica could be harvested directly from genetically engineered organisms.[41,42] Using the biomimetic approach, it has been demonstrated recently that mono- and polyamines have the ability to catalyze silica precipitation at near-neutral pH.[26−36,43−46] The effectiveness of the amine as a catalyst appears to be dependent on the isoelectric point of the amine[28,35,43] and, therefore, possibly the concentration of the amine conjugate base. Although it is unknown how diatoms and sponges store silica intracellularly prior to precipitation at concentrations exceeding silica solubility, small silicate oligomers and organosilicate compounds have been hypothesized as precursors.[42,47] In the present study, we use ^{29}Si NMR spectroscopy and ab initio computational methods to investigate the role of amines in the chemical mechanisms of organosilicate hydrolysis at circum-neutral pH.

Previous computational studies have demonstrated that organosilicate hydrolysis can occur through a mechanism involving a pentacoordinate intermediate, similar to those found in the S_N2 mechanism, under acidic or basic conditions.[20,23−25] In the presence of strongly nucleophilic amines, however, an alternative mechanism for hydrolysis was proposed by Corriu. This mechanism (Figure 1), termed "nucleophile-activated (N_a) nucleophilic (N_b) substitution" [48,49] (hereafter called nucleophile-activated substitution) was invoked to account for rapid precipitation/gelation of silica in the presence of weakly basic nucleophiles such as amines.[48] In this mechanism, hydrolysis is initiated by coordination of the nucleophile (N_a) to silicon to form a pentacoordinate intermediate. A hexacoordinate transition structure is then formed as water (the substituting nucleophile, N_b) attacks the silicon center. Hydrolysis is completed once the leaving group and the nucleophile (N_a) break away from silicon, the nucleophile (N_a) abstracting a proton from water (N_b) as it

* Corresponding author. E-mail: kd33@nyu.edu. Tel: (608)265-5192. Fax: (608)262-0693.
† Department of Chemistry, University of Wisconsin, Madison.
‡ Current Address: New York University, Department of Chemistry, 100 Washington Square East, Room 1016, New York, NY 10003. Tel: (212)988-8442. Fax: (212)260-7905.
§ Department of Geology & Geophysics, University of Wisconsin, Madison.

10.1021/jp062054m CCC: $33.50
Published on Web 08/22/2006

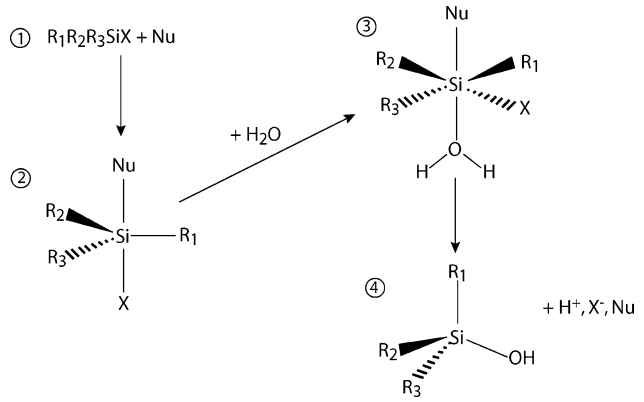

Figure 1. Mechanism for nucleophile-assisted nucleophilic substitution as proposed by Corriu, where Nu is the nucleophile and X is the leaving group.

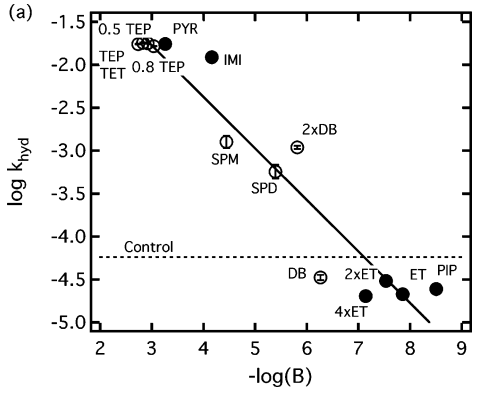

Figure 2. Dependence of TMES hydrolysis rates (k_{hyd}) on amine conjugate base concentration. The slope is 0.60 ± 0.05, with R^2 = 0.9612. Reproduced with permission from *Chem. Mater.* **2005**, *17*, 4272. Copyright 2005 American Chemical Society.

leaves. Although this mechanism was never explicitly proven via experiment, strong evidence for it was provided based on the stereochemical retention of halogenosilane substitution products in the presence of nucleophiles[50,51] and the evolution of H_2 gas in the alcoholysis of $[HSi(OR)_4]^-$ K^+ by a weak base.[52]

Here we examine the hypothesis that amines may act to promote hydrolysis of model organosilicates via a nucleophile-assisted mechanism, based on our previous results that hydrolysis and condensation rates of trimethylethoxysilane (TMES) at mildly acidic pH (~6) were proportional to the conjugate base concentration of the amine (Figure 2).[35] Of the amines tested, those with low pK_a values had the largest conjugate base concentration at mildly acidic pH and are typically the most nucleophilic. Further support for amine-catalyzed nucleophile-assisted hydrolysis is based on preliminary ab initio studies that demonstrated that stable pentacoordinate structures of amines bound to the silicon center of trimethoxyserinesilicate (Ser-O−$Si(OCH_3)_3$) could exist.[53] In these structures, the Si−O bond distances were lengthened up to 1.73 Å, suggesting that coordination of a nucleophile to silicon may result in a pentacoordinate structure where steric crowding about silicon is relieved sufficiently so that water can attack.

In detail, we examine the hydrolysis of trimethlyethoxysilicate (TMES) as catalyzed by tetraethylenepentamine (TEP) and pyridine (PYR) over a range of pH values, and spermidine (SPD) and imidazole (IMI) at pH ≈6 over a broad temperature range. The amines are selected from a longer list of mono- and polyamines used in our previous study of hydrolysis rates, and represent different nitrogen atom hybridizations and reactivities. Also, IMI and TEP represent the chemical functionalities of histidine and polylysine, amino acid residues found in the active sites of the silica precipitating proteins of the sponge *T. aurantia*[39] and of various diatoms.[37,38]

Our choice of TMES and TMOS as model organosilicate precursors was driven by both practical and theoretical considerations. Numerous ^{29}Si NMR kinetic studies of organosilicate hydrolysis and condensation at extreme pH values have been carried out using tetrafunctional organosilicates,[5,6,14−16] but thorough evaluation and modeling of the system proves to be extremely demanding because of multiple potential hydrolysis, re-esterification, oligomerization, and rehydrolysis steps. Consequently, to evaluate the catalytic effect of a number of amines over a range of conditions using a tetrafunctional organosilicate would be a monumental task! We, therefore, chose to use TMES because it is a monofunctional organosilicate with only a single reactive bond. As such, the chemical influence of amines on kinetics can be evaluated easily, while eliminating any complications that may arise from phase separation or cyclization.

In the ab initio portion of our study, we use both TMES and TMOS as model organosilicates. In doing so, we explore the contrast between TMES, an organosilicate where silicon is less electrophilic because of the presence of three electron-donating methyl groups, and TMOS. We, therefore, evaluate the differences in nucleophilic mechanisms between these two precursors.

The reaction mechanisms were explored computationally using an approach based on Hammond's postulate, where we calculated the geometry and energy of putative intermediates close to the actual transition states along the proposed reaction pathways.[54] The computational results for TMES were combined with experimental studies examining the pH and temperature dependence of TMES hydrolysis. Although the mechanism of nucleophile-activated hydrolysis has been investigated for silatranes,[55−57] these studies present the first examination of the *chemical* mechanism by which *free* amines may act to hydrolyze silicate precursor compounds.

Methods

Kinetic Studies. The experimental details of the ^{29}Si NMR rate studies have been described previously.[35,58] In short, a 4 M ethanolic solution of TMES (Gelest, twice distilled) was combined in equal parts with an ethanolic solution that was 8 M in H_2O and 2 mM in amine, so the final concentrations of reagents in the reaction were 4 M H_2O, 2 M TMES, and 1 mM amine. The pH was set by titrating acid or base into an aqueous amine-containing stock solution. This solution was then diluted with ethanol (1−10 mL) to make the catalyst-containing ethanolic solution.

NMR spectra were acquired using the RINEPT+ pulse sequence[58,59] because we had found previously that the presence of paramagnetic relaxation agents affected hydrolysis rates.[59] Spectra were obtained with parameters set using a J_{H-Si} of 6.9 Hz on a Varian UNITY spectrometer with a broad-band probe operating at 99.326 MHz on the ^{29}Si channel and proton decoupling centered at 499.625 MHz. Relaxation times (T_1 and T_2) were measured over a broad temperature range to verify the quantitative accuracy of the experiment and set the delay time appropriately.[60,61] Variable-temperature experiments were conducted using 2 steady-state scans, 4 transients per spectrum, and 20 s between spectra, and were run for approximately 20 min. Samples were thermostated using ice water, dry ice and ethylene glycol, or dry ice and acetone baths prior to insertion into the spectrometer. The temperature in the spectrometer was

verified using a methanol standard.[62] Studies of hydrolysis pH dependence were carried out using 2 steady state scans, 8 transients per spectrum, and an increase of 30 s between spectra (i.e., 30, 60, 90, 120 s) and were run for at least 8 h. All spectra were obtained without a lockable solvent, but spectral acquisition times were sufficiently short (~75 s) such that line broadening from shifting of peaks during acquisition was not a concern. Data were obtained from spectra through routine integration with normalization of peak integrals using VNMR software. Concentrations of material present were then calculated based on the initial amount of starting material using the normalized integral values from each spectrum.

The amines used for the variable-temperature study included imidazole (IMI, Aldrich 99+%) and spermidine (SPD, Fluka ≥ 99%). These amines were chosen because hydrolysis proceeds at an intermediate rate,[35] enabling easy quantification of rate constants. In addition to experiments with amine catalysts, control samples were prepared where HCl was added to achieve a pH (≈6) that corresponded to the pH in the amine-containing samples, and an additional control at pH ≈ 5 to verify that hydrolysis of the control sample was proceeding by acid-catalysis. These are referred to as the "strong acid controls" throughout the text, where the term "strong acid" refers to the ability of HCl to dissociate completely in solution, and not its concentration.

Pyridine (PYR: Acros ACS reagent grade) and tetraethylenepentamine (TEP: Aldrich, technical grade) were used to study the dependence of hydrolysis on pH because these amines were shown to be superior in catalyzing hydrolysis and condensation,[35] so it was assumed that pH effects would also be more pronounced.

Computational Methods. Geometry optimizations and energy calculations were conducted using the Gaussian 03 software package[63] at the B3LYP/6-31G(d) level.[64−66] The hybrid density functionals combine some SCF exchange with DFT electron correlation and exchange, and often result in overestimation of bond lengths, but B3LYP is used commonly in the study of silicon systems and is a better predictor of hydrogen-bonding effects.[57,67]

Attempts to determine the reaction pathway using synchronous transit (STQN) methods, as well as the method of constrained optimization along potential reaction paths,[68] were unsuccessful, primarily because true transition states could not be identified, and because the geometric contortions required for formation of the structures were not conducive to STQN methods. We, therefore, used geometry optimizations to obtain structures and energies of stable intermediates to construct the pathway. According to Hammond's postulate, the stable intermediates should resemble transition states that are close in energy if the two structures occur consecutively in a reaction.[54] Thus, the calculated reaction energies for each elementary step in the overall pathway are assumed to correspond closely to activation energies. The amines studied computationally included PYR, IMI, and ethylamine (ET). TEP could not be studied computationally because of prohibitive computational costs. Energies were corrected for thermal contributions and were used to compare the stability of the various reactants, intermediates, and products. Solvation effects on geometries were initially considered by conducting calculations using both COSMO and CPCM continuum solvation models. These had no appreciable qualitative effect on geometry. We, therefore, considered solvation by the explicit inclusion of up to three water molecules.

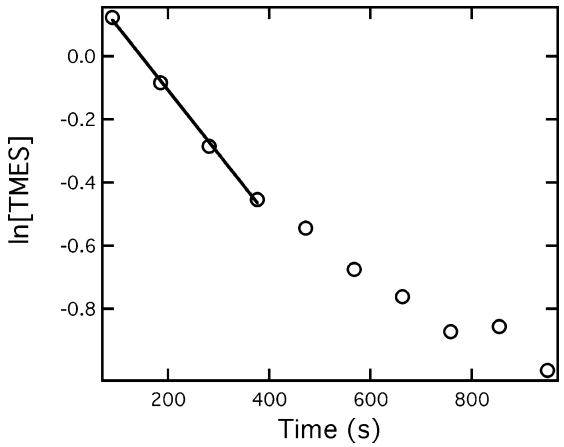

Figure 3. Plot of ln[TMES] vs time for imidazole-catalyzed TMES hydrolysis at 0 °C. A straight line is fit to the linear portion of the graph to obtain rate constants for hydrolysis.

Results

Rate Constants from NMR Experiments. The reactions for TMES hydrolysis and condensation are detailed in Scheme 1.

SCHEME 1: Trimethylethoxysilane Hydrolysis, Followed by Either Water Condensation or Ethanolic Condensation Paths

$$(CH_3)_3SiOCH_2CH_3 + H_2O \rightarrow (CH_3)_3SiOH + CH_3CH_2OH \quad (1)$$

$$(CH_3)_3SiOH + (CH_3)_3SiOH \rightarrow (CH_3)_3SiOSi(CH_3)_3 + H_2O \quad (2a)$$

$$(CH_3)_3SiOH + (CH_3)_3SiOCH_2CH_3 \rightarrow (CH_3)_3SiOSi(CH_3)_3 + CH_3CH_2OH \quad (2b)$$

Both the decrease in TMES concentration and the increase of the hydrolyzed product are indicators of hydrolysis rates because condensation does not begin until hydrolysis is complete. Here we follow TMES concentrations.

A representative plot of ln[TMES] versus time as catalyzed by IMI at 0 °C shows a linear trend during the initial hydrolysis period, suggesting a first-order reaction (Figure 3). For the purpose of quantifying k_{hyd}, we considered only the linear portion of the fit and obtain pseudo first-order rate constants for TMES hydrolysis. This contrasts with our previous study where we plotted TMES concentration versus time.[35] More data points, however, can be included in the linear trend of ln[TMES], allowing for better quantification of the hydrolysis rate constant (k_{hyd}). Deviation from linearity begins once the reaction approaches what has been termed "hydrolysis pseudoequilibrium" at which point the reverse of hydrolysis (esterification) becomes significant.[59] Condensation rate constants (k_{cond}), where reported, were obtained by fitting a straight line to the inverse of the total monomer concentration.[35,59]

pH Dependence. The hydrolysis and condensation rate data for PYR and TEP with respect to pH are shown in Figure 4a and b, and in Table 1. At low pH, our ability to measure the hydrolysis rate was limited by the temporal resolution of the NMR experiment, so the data at pH 4 and pH 5.8 are not quantitatively accurate. However, because condensation does not begin until hydrolysis is nearly complete, its rate is dependent on and directly related to the hydrolysis rate. We, therefore, have included for these two pH conditions the results showing the dependence of the condensation rate on pH.

The hydrolysis rate constants increase steadily for both PYR and TEP with decreasing pH. The inverse relationship between the reaction rates and pH suggests either proton-promoted

TABLE 1: Rate Constants for pH Dependence of TMES Hydrolysis and Condensation, at 26°C

catalyst	pH 4	pH 5.8	pH 7.6	pH 9.8
		hydrolysis (k_{hyd} in 10^{-3} s^{-1})		
pyridine	13.3 ± 0.4	13.0 ± 0.3	0.460 ± 0.002	0.0065 ± 0.0005
tetraethylenepentamine	12.4 ± 0.1	12.9 ± 0.3	0.008 ± 0.002	0.0002 ± 0.0001
		condensation (k_{cond} in 10^{-5} L mol^{-1} s^{-1})		
pyridine	40 ± 10	6 ± 2	0.50 ± 0.03	[a]
tetraethylenepentamine	13.00 ± 0.01	3.1 ± 0.1	[a]	[a]

[a] Condensation rates were too slow to be observed within the time frame of the experiment.

TABLE 2: Hydrolysis Rate Constants (units of 10^{-4} s^{-1}) Obtained from Variable-Temperature Experiments

temperature	HCl pH 6.05	imidazole	spermidine	temperature	HCl pH 5.16
23 °C	0.32 ± 0.03	134 ± 4	14 ± 4	23 °C	2.9 ± 0.3
0 °C	0.11 ± 0.02	19.1 ± 0.9	3.6 ± 0.3	5 °C	2.0000 ± 0.0008
−12 °C	0.07 ± 0.02	11.7 ± 0.6	1.7 ± 0.3	−30 °C	0.26 ± 0.03
−32 °C	0.03 ± 0.0007	3.56 ± 0.09	0.048 ± 0.002		
−56 °C	[a]	0.19 ± 0.02	[a]		
activation energy (kJ mol^{-1})	24 ± 2	42 ± 3	37 ± 1		28 ± 4

[a] Data not obtained at this temperature.

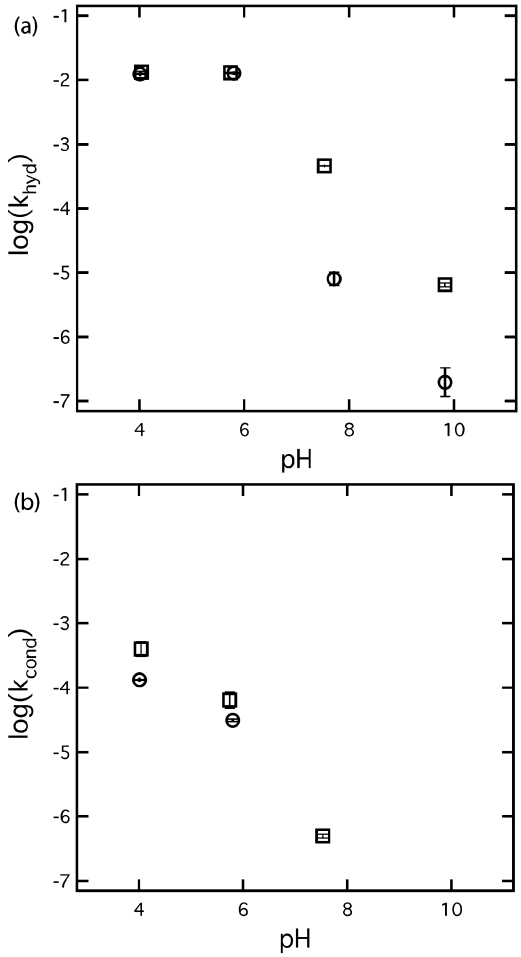

Figure 4. Dependence of TMES (a) hydrolysis and (b) condensation on pH. Rates with both pyridine (square) and tetraethylenepentamine (circle) as catalysts increase with acidity.

hydrolysis without the involvement of amines in catalysis or that the conjugate acid form of the amine is the primary factor contributing to catalysis of TMES hydrolysis. These results contrast directly with our previous observation that, at constant pH ≈ 6.5, hydrolysis and condensation rates are related to the concentration of the amine in its conjugate base form.[35]

Experimental Determination of Activation Energy. Activation energies were calculated from variable-temperature studies using the Arrhenius equation

$$k = A \exp -(E_{act}/RT)$$

where A is a preexponential frequency factor, E_{act} is the activation energy, R is the gas constant (8.314 J mol^{-1} K^{-1}), and T is the temperature in Kelvin. The individual rate constants from our experiments are summarized in Table 2. The apparent activation energies found for the amine-catalyzed reactions are actually higher than those for the strong acid controls. The control at pH 6.05 and its more acidic complement at pH 5.16 have activation energies that are within error, indicating that hydrolysis proceeds through the same acid-catalyzed mechanism at both pH values. The activation energy for TMES hydrolysis by imidazole, the more effective of the two amine catalysts, is higher than that for spermidine. These results run contrary to the classical definition of a chemical catalyst, which is an agent that increases the reaction rate by providing an alternative pathway for the reaction that has a *lower activation energy*.[69]

Calculations. In the amine-catalyzed hydrolysis of TMES, nucleophiles available for reaction include water, ethanol (the solvent), and amines. To assess whether the amine-catalyzed nucleophile-activated substitution mechanism was viable, we attempted to identify stable pentacoordinate intermediates of pyridine, imidazole, and ethylamine binding directly to TMES, similar to those in Figure 1. Gas-phase pentacoordinate or pseudo-pentacoordinate silicon complexes, with distorted trigonal-bipyramidal geometries, were obtained only when the ethoxy group was protonated and axial to the amine (Figure 5a). The Si−O bond lengths range from 2.36 to 3.73 Å, the higher number corresponding closely to the sum of van der Waals radii for silicon and oxygen (3.62 Å). Silicon−nitrogen bond lengths are correspondingly shorter, with values ranging from 1.8 to 2.0 Å (Table 3). The only true pentacoordinate complex obtained was for ethylamine. Explicit solvation of the complexes through the addition of three water molecules resulted in shortening of the bond distances, particularly in the silicon−pyridine complex, where the Si−O bond lengths are truncated in comparison to the solvated case. In both the solvated and unsolvated systems, the Si−N bond lengths fall into the range found in silatranes[70] (Figure 5b).

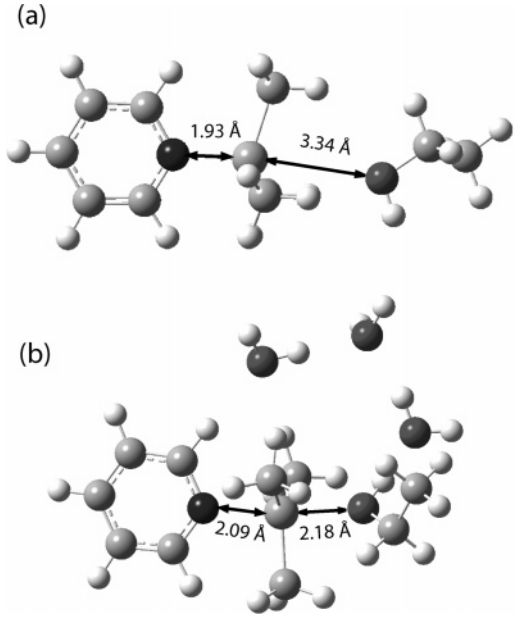

Figure 5. Optimized structures of pyridine with TMES without (a) and with (b) explicit solvation. Bond distances for structures are found in Table 3. The third methyl group in part a is hidden from view by another methyl group in front of it.

TABLE 3: Bond Distances (Å) from Optimized Pseudo-Pentacoordinate and Pentacoordinate Structures of TMES with Amines

	without solvating waters		with three solvating water molecules	
amine	Si−N	Si−O	Si−N	Si−O
pyridine	1.9333	3.34089	2.09057	2.17822
imidazole	1.80365	3.73392	1.90213	3.18052
ethylamine	2.02503	2.36524	2.05449	2.15765
acid/water	2.25520	2.00398		

The shortened bond distances observed in explicitly solvated complexes led us to believe that under the proper solvation conditions a pentacoordinate complex may be observable spectroscopically. As with previous studies,[52] our attempts to identify such a complex using XPS (vacuum), ^{15}N NMR with enriched samples, ^{29}Si NMR, and attenuated total reflection (ATR) FTIR spectroscopies were, however, unsuccessful. We were also unable to locate a hexacoordinate intermediate or transition state through geometry optimizations, as well as by STQN (quadratic synchronous transit) methods in Gaussian 03.[63]

We, therefore, examined two alternative reaction pathways, one involving the direct coordination of the amine to silicon (Figure 6a) and a second in which the amine acts solely as a proton-transfer agent to facilitate S_N2 hydrolysis (Figure 6b). The enthalpies of all of the intermediate components along each reaction pathway were calculated (Table 4), and the results for imidazole are plotted in Figure 6c. Surprisingly, the protonation of TMES by the amine is energetically the most costly step of the reaction in both cases so that there is no energetic advantage of one pathway over the other. Again, we were unable to obtain any spectroscopic evidence of direct coordination between the amine and silicon.

We also examined the possibility of TMOS hydrolysis occurring through Corriu's nucleophile-activated substitution. Stable penta- and hexacoordinate complexes of ethylamine, pyridine, and imidazole with TMOS were identified, and the critical bond lengths are listed in Table 5. For the pentacoordinate complexes, contrary to expectation, binding of the amines in these complexes occurs at the equatorial position rather than

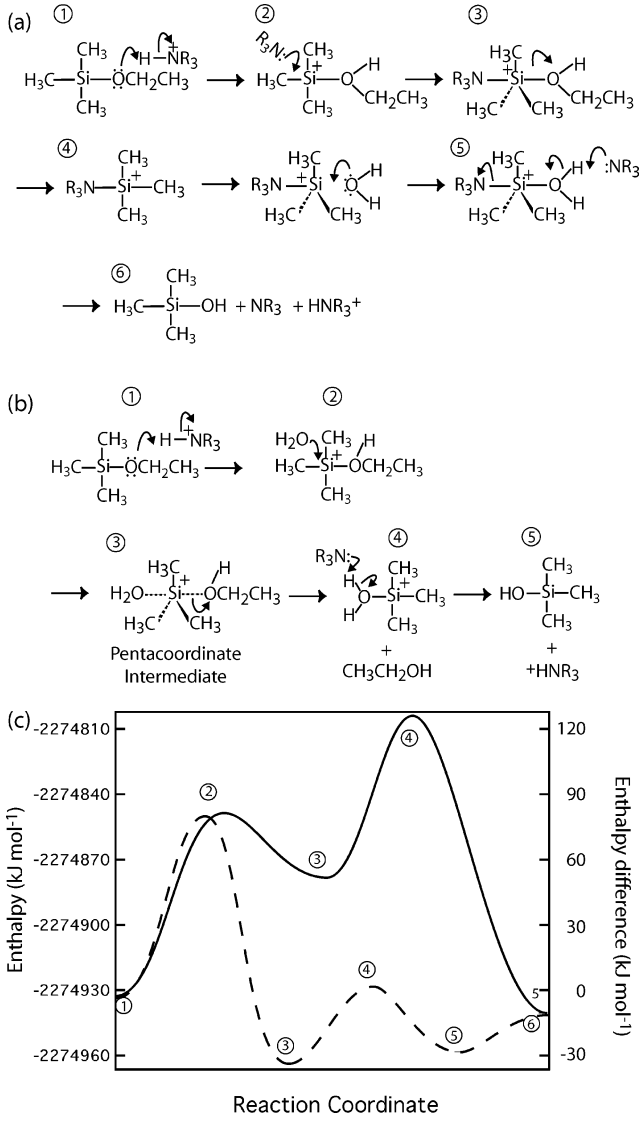

Figure 6. Possible reaction mechanisms for TMES hydrolysis including direct binding of the amine to TMES (a) and S_N2 hydrolysis with the amine as a proton-transfer agent (b). The pathways in terms of potential energies are shown in (c) where the dashed line corresponds to the mechanism in (a) and the solid line corresponds to (b).

the axial position observed in silatranes (Figure 7a). The exception is ethylamine, which is capable of binding at both the equatorial and axial sites. The isomer in which ethylamine is axially bound is approximately 40 kJ mol^{-1} lower in energy than the equatorially bound one. The structures of the hexacoordinate compounds correspond to that in Figure 1, and water is bound in a position trans to the amine (Figure 7b). Enthalpies for the steps of the nucleophile-activated hydrolysis pathway as well as the proton-transfer pathway were calculated from the geometry optimizations (Table 6) and are plotted in Figure 8.

Discussion

Reaction Mechanisms. The computational result that (pseudo)-pentacoordinated TMES complexes were obtained only when the ethoxy group was protonated indicates that protonation of the ethoxy group in TMES is a required step in both of the mechanisms explored here. If the proton-transfer step were followed by direct binding of the amine to TMES, then we would anticipate that the reaction rate would be fastest at the pK_a of the amine catalyst, where concentrations of conjugate acid and base are equal. This is not observed experimentally.

TABLE 4: Enthalpies (kJ mol^{-1}) for S_N2 Pathway for TMES Hydrolysis (Top) and with Direct Binding of Amine Conjugate Base as Catalyst (Bottom) Relative to the Energy of the Initial Reactants[a]

catalyst	(1) catalystH$^+$ TMES, H_2O	(2) TMESH$^+$ catalyst, H_2O	(3) pentacoordinate intermediate, catalyst	(4) hydrolyzed TMESH$^+$ catalyst, ethanol	(5) catalystH$^+$, ethanol, hydrolyzed TMES
acid	0.00	−174.60	−203.25	−129.61	−7.35
ethylamine	0.00	51.61	22.96	96.60	−7.35
imidazole	0.00	82.89	54.23	127.88	−7.35
pyridine	0.00	67.85	39.19	112.84	−7.35

catalyst	(1) catalystH$^+$ TMES, H_2O	(2) TMESH$^+$ catalyst, H_2O	(3) 5-coordinate TMESH$^+$ amine adduct, H_2O	(4) R3N:Si$(CH_3)_3^+$, H_2O, ethanol	(5) 5-coordinate TMSiOH_2^+ amine adduct, ethanol	(6) catalystH$^+$ ethanol, hydrolyzed TMES
ethylamine	0.00	51.60	−24.59	1.77	−41.21	−7.35
imidazole	0.00	82.89	−30.48	4.34	−25.24	−7.35
pyridine	0.00	67.85	−14.39	12.43	−16.33	−7.35

[a] Numbers in parentheses refer to corresponding intermediates and transition states in Figure 6a and b.

TABLE 5: Bond Distances (Å) from Optimized Pentacoordinate and Hexacoordinate Structures of TMOS with Amines

	pentacoordinate			hexacoordinate	
amine	Si−N	Si−O (axial)	Si−O (equatorial)	Si−N	Si−O (water)
imidazole	2.06182	1.725	1.68	1.95637	2.18174
pyridine[a]	1.95	1.73	1.68	1.99867	2.14682
ethylamine	2.07351	1.725	1.67	1.98541	2.15672

[a] Bond distances are to two decimal places only because this stable geometry was obtained as part of an incremental process in a relaxed potential energy surface scan.

Instead, pH-dependent behavior is seen where hydrolysis rates increase with decreasing pH, which is consistent only with the S_N2 mechanism.[6,16,71] Second, the calculated activation energy trends for the S_N2 mechanism follow those obtained experimentally and correspond to ethoxy-group protonation (Table 7). Furthermore, the lack of spectroscopic evidence of compounds where the amine binds directly to silicon provide further indication that proton transfer, coupled with S_N2 hydrolysis, is most likely the dominant mechanism.

The present result apparently contradicts our earlier result where reaction rates were faster in the presence of amines relative to the strong acid control. The contradiction, however, can be clarified if we take into account that the reaction rate depends on both concentration and E_{act} of the catalyst. At pH 6 and 1 mM amine, the solution contains up to 3 orders of magnitude greater proton concentration associated with the conjugate acid form of the amine than the corresponding strong acid solution. In other words, our previous observation that amine catalysis is proportional to the conjugate base concentration was simply an indicator of the fact that amines that are strongly basic do not surrender their protons to TMES as easily as amines with lower pK_as. Consequently, hydrolysis with strongly basic amines at near-neutral pH proceeds much more slowly. On a per-mole basis, the strong acid is a far more effective catalyst for TMES hydrolysis than the amines, as seen by the faster acid-catalyzed rates at lower pH.

Results from the present study raise questions about the role of the amine. Do amines act simply as protonating agents that create a better leaving group and thus facilitate S_N2 hydrolysis, or does hydrolysis occur through some alternative mechanism such as nucleophile-activated substitution? Furthermore, is the role of amines similar for all organosilicates? The case for

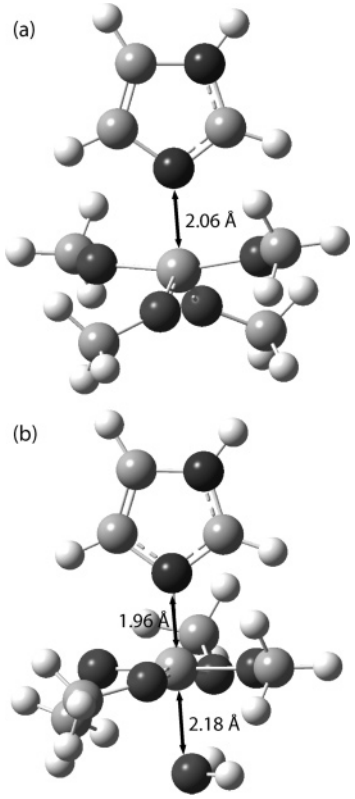

Figure 7. Optimized pentacoordinate structure of TMOS with imidazole (a) and hexacoordinate structure of TMOS, imidazole, and water (b).

organosilicate hydrolysis via nucleophilic-activated substitution was first made based on the observation that TMOS gelled more quickly in the presence of dimethylamino pyridine (DMAP) and *N*-methyl imidazole (NMI) than in a comparable amount of acid.[48] Both of these strong nucleophiles are known to activate silicon through pentacoordination in organsilicon reactions. Likewise, the reaction products of halosilanes with nucleophiles such as dimethylformamide exhibited stereochemical retention, suggesting that substitution reactions did not proceed through a standard S_N2 reaction involving a pentacoordinate intermediate, but rather through some alternative pathway that involved a highly organized transition state.[50,51] Moreover, pentacoordinate, anionic organosilicates, where the starting material includes a precoordinated nucleophile already bonded to silicon, pre-

TABLE 6: Enthalpies (kJ mol^{-1}) for the S_N2 Pathway for TMOS Hydrolysis (Top) and for Nucleophile-Activated Substitution Hydrolysis of TMOS (Bottom) Relative to the Energy of the Initial Reactants[a]

catalyst	(1) catalystH$^+$ TMOS, H_2O	(2) TMOSH$^+$ catalyst, H_2O	(3) pentacoordinate intermediate, catalyst	(4) hydrolyzed TMOSH$^+$ catalyst, methanol	(5) catalystH$^+$ methanol, hydrolyzed TMOS
acid	0.00	−142.61	−193.38	−111.95	−6.23
ethylamine	0.00	83.60	32.82	114.25	−6.23
imidazole	0.00	114.88	64.10	145.53	−6.23
pyridine	0.00	99.84	49.06	130.49	−6.23

catalyst	(1) amine, TMOS, H_2O	(2) 5-coordinate, H_2O	(3) 6-coordinate	(4) amine, hydrolyzed TMOS, methanol
ethylamine	0.00	73.56	97.47	−6.23
imidazole	0.00	74.88	90.67	−6.23
pyridine	0.00	99.66	104.86	−6.23

[a] Numbers in parentheses refer to the intermediates and transition states in the S_N2 mechanism, similar to that shown in Figure 6b and in Corriu's scheme as depicted in Figure 1.

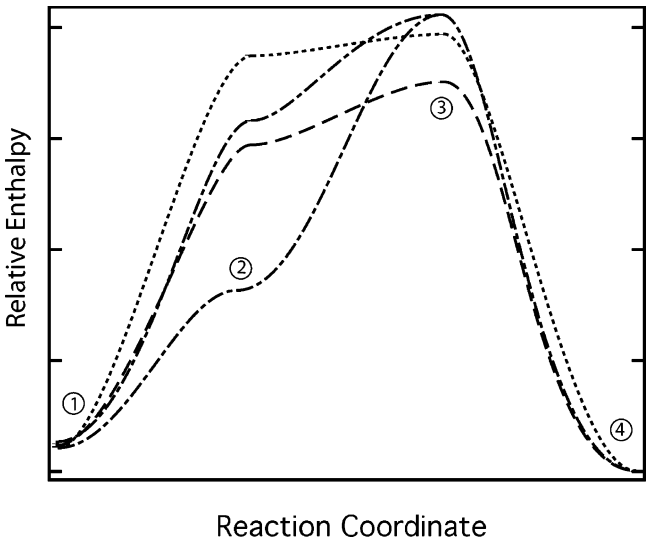

Figure 8. Reaction pathway in terms of potential energy for nucleophile-assisted substitution for TMOS hydrolysis by pyridine (short dashes), ethylamine (short and long dashes), and imidazole (long dashes). Enthalpies are shown relative to the lowest energy species [1 − (energy/minimum energy)]. Graphs of the proton-transfer S_N2 mechanism with the amines are not shown but are similar in profile to those for TMES (solid line in Figure 6c). Numbers correspond to molecular structures in Figure 1, except the pentacoordinate structures for imidazole and pyridine have the amine bound at the equatorial site. Relative enthalpies for both the axially and the equatorially bound pentacoordinate ethylamine-TMOS adduct are shown.

TABLE 7: Activation Energies for TMES Hydrolysis from Variable-Temperature Experiments and from Calculations[a]

catalyst	protonation of TMES (S_N2), calculated	experimental	R^2	preexponential factor
imidazole	82.89	42 ± 3	0.9922	13 ± 1
spermidine	51.61[b]	37 ± 1	0.9990	8.3 ± 0.5
HCl pH 6.05	−174.60	24 ± 2	0.9947	−0.6 ± 0.8
HCl pH 5.16	−174.60	28 ± 4	0.9877	3 ± 2

[a] All values are in kJ mol^{-1}. [b] Ethylamine is used as a computational proxy for spermidine.

cipitated silica much more rapidly than their tetracoordinate counterparts.[52] Because both DMAP and NMI are strong nucleophiles that can form pentacoordinate silicon species, nucleophile-activated catalysis appeared to be the most plausible mechanism for the hydrolysis process.[48]

The possibility of hydrolysis proceeding through a nucleophile-activated substitution appears to be related directly to a nucleophile's ability to form a complex where silicon is pentacoordinated. Pentacoordinate silicon compounds with amines are commonly found in silatranes and are characterized by a trigonal-bipyramidal geometry where the amine occupies the axial position.[49,70] The silicon−nitrogen bond is, typically, a weak dative bond that is highly sensitive to inductive effects, particularly from the equatorial groups.[72] For instance, Si−N bond distances are approximately 0.79 Å longer for $RSiMe_3$ compounds than $RSiF_3$ compounds.[49] The nucleophilicity of the amine, as well as the inductive character of the substituent trans to the amine are additional factors that contribute to the strength of the Si−N bond.[72−75] We would, therefore, anticipate that formation of a stable pentacoordinate intermediate with TMOS is much more likely than that with TMES because silicon is more electrophilic in TMOS.

As expected, our geometry optimizations show that both penta- and hexacoordinate complexes of amines with TMOS were stable, whereas corresponding structures with TMES were not. The TMOS structures corresponded to those suggested by Corriu,[48] except that the amine is bound to silicon at the equatorial site rather than the anticipated axial site in the pentacoordinate complexes. This geometry is intuitively sensible if one considers the amount of distortion required in the complex to accommodate water in the subsequent hexacoordinate structure. Water is found trans to the amine in the hexacoordinate structure (Figure 6b). When the amine is bound at the equatorial site, the distortion requires only a widening in the angle between the two equatorial methoxy groups, corresponding to a wagging vibrational motion that is observed computationally for all three amine complexes. However, a greater distortion is required to accommodate water when the amine is axially bound. This geometric argument is also supported by energetic results, where the axially bound ethylamine complex is 40 kJ mol^{-1} lower in energy than the equatorially bound isomer. Once the hexacoordinate structure is formed, hydrolysis is expected to proceed via a transition state in which a proton from water is transferred to the methoxy group. Though not explicitly shown here, this mechanism was demonstrated computationally for hydrolysis of silatranol by Chernyshev.[57]

The activation energies for the mechanism of nucleophile-activated catalysis are generally comparable to those for hydrolysis via proton transfer followed by the S_N2 reaction (Table 8). Of interest is the fact that S_N2 hydrolysis is the

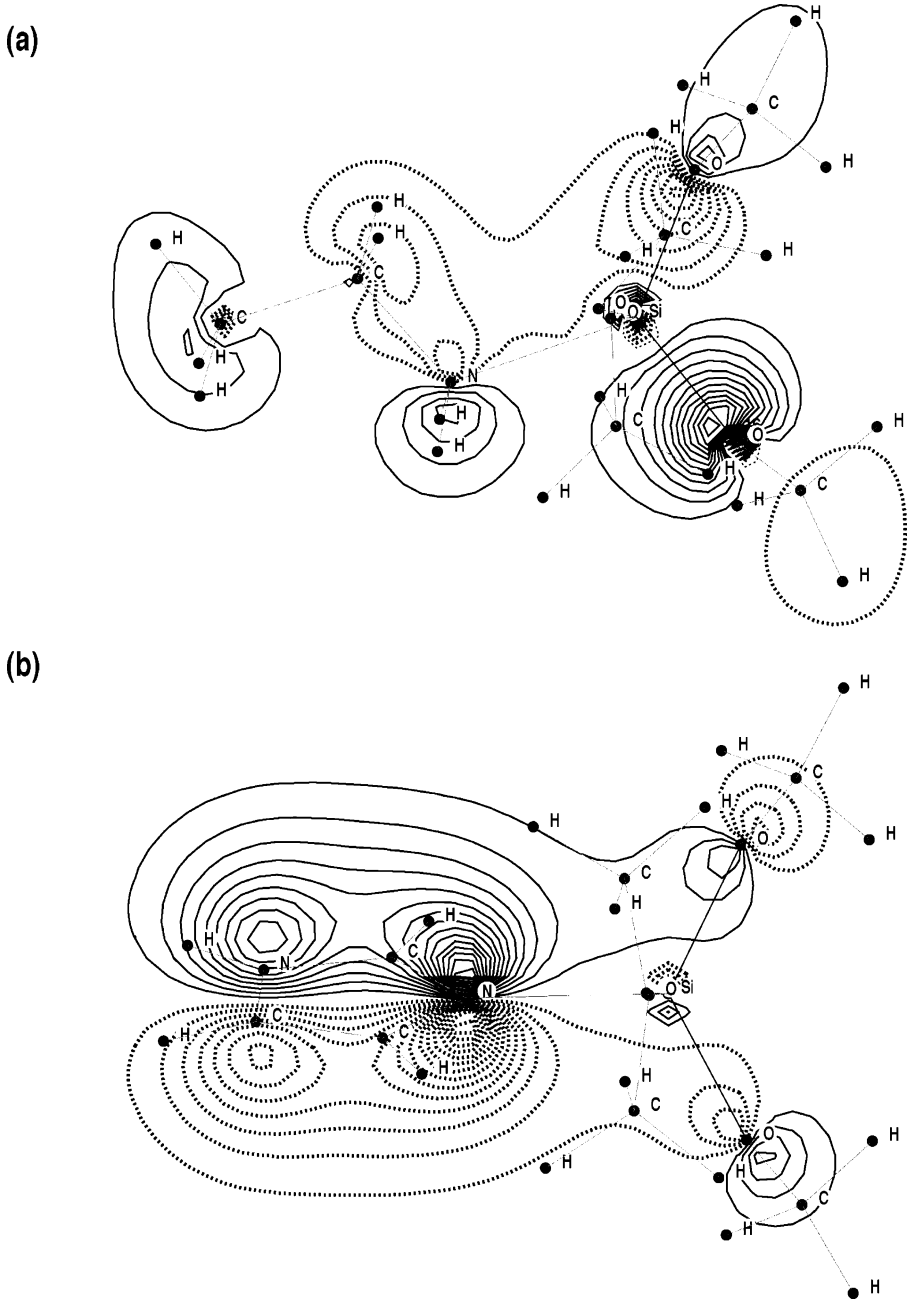

Figure 9. Molecular orbitals depicting π-interaction between the *p*-type oxygen orbitals of TMOS and those of the amine nitrogen. The long axis of the trigonal-bipyramidal structure is perpendicular to the page. The orbitals shown are molecular orbital 25 in ethylamine (a), and molecular orbital 36 for imidazole (b). Contour spacing is 0.0125. Figure produced using MOLDEN.[86]

TABLE 8: Calculated Activation Energies (kJ mol^{-1}) of TMOS Hydrolysis from for the S_N2 Pathway Where the Amine Is a Proton-Transfer Agent, and for Nucleophile-Assisted Catalysis

catalyst	protonation of TMOS (S_N2)	nucleophile-assisted catalysis
imidazole	114.88	90.67
ethylamine	83.60	97.46
pyridine	99.84	104.86
acid	−142.61	

preferred pathway for ethylamine by ∼14 kJ mol^{-1}, whereas nucleophile-activated catalysis is favored for imidazole by ∼24 kJ mol^{-1}. The slightly higher energetic cost of the equatorially bound ethylamine adduct over the axially bound conformation likely contributes to the higher activation energy for nucleophile-activated catalysis than for S_N2 catalysis. Further insight can be gained by examination of comparable molecular orbitals (MOs) in the square-pyramidal TMOS complexes for ethylamine and imidazole (Figure 9). Molecular orbital 25 for the ethylamine structure and MO 36 for the imidazole structure both contain *p*-type orbitals on oxygens that combine with a *p*-type orbital on nitrogen, resulting in a π-type molecular orbital that helps to bring the nitrogen in close proximity to the central silicon atom of TMOS. Inspection indicates that the planarity of the π-conjugate system in imidazole allows for a more symmetrical structure in which the orbital overlap is enhanced over that in ethylamine. We see, therefore, that the hybridization of the amine nitrogen along with the accompanying π-conjugate system found in imidazole contributes to a greater stability of the pentacoordinate structure and accounts for the lower activation energy of the nucleophile-activated hydrolysis mechanism.

Relevance to Sol−Gel Silica Synthesis. Our conceptual arguments suggest the possibility of hydrolysis through the nucleophile-activated substitution mechanism for TMOS. It would appear, therefore, that different factors determine the pathway for hydrolysis. In all of the cases examined computationally, the difference in activation energies between the S_N2 mechanism and nucleophile-activated catalysis is no greater than ~24 kJ mol^{-1}. As such, a major factor contributing to the mechanism driving hydrolysis is pH. Where pH > pK_a, nucleophile-activated catalysis is likely favored because the amine exists predominantly in the conjugate base form. For pH < pK_a, S_N2 catalysis is favored. The exception is ethylamine; its axially bound pentacoordinate isomer is energetically favored and could therefore prevent hydrolysis from occurring through the nucleophile-activated mechanism where the equatorially bound structure is necessary. This, in conjunction with the high pK_a of ethylamine, leads us to believe that ethylamine acts via the proton-transfer mechanism over a wide range of pH values.

The type of orthosilicate and the electrophilicity of silicon in the organosilicate is also significant in determining the catalytic pathway. The presence of electron-donating groups bonded to silicon, such as the methyl groups in TMES, does not appear to allow for the nucleophile-activated mechanism at all. Presumably, in TMOS, the silicon is more electrophilic because of the electron-withdrawing tendencies of the four methoxy groups bound to it. The pentacoordinate structure necessary for nucleophile-activated catalysis is, therefore, favored in organosilicates where silicon is more electrophilic.

Finally, sp^2-hybridized amines with geometries that allow for the enhancement of π-orbital overlap appear to be significant in promoting nucleophile-activated catalysis as a potential hydrolysis pathway.

Relevance to Biological Silica Synthesis. We may now examine the potential biological relevance of our results. First, the manner in which silica is solubilized by diatoms and sponges prior to precipitation is unknown and appears to be species-dependent.[42] Silica may be stored in vesicles or dispersed throughout the cytoplasm, but in both cases the concentrations of silica exceed the solubility of silicic acid.[42,47] It has been hypothesized that silica precursors exist as organosilicates such as silicon-catechol compounds, sugar−silicate complexes, or octasilsesquioxane-like compounds, all of which can exist at concentrations significantly higher than the solubility limit of silicic acid. Synthesis of sugar silicates from common biologically occurring sugars [76] and low-temperature isolation of ammonium silsesquioxanes ($[OSiO_{1.5}]_8[R_4N]_8$) [77] have been accomplished successfully in the laboratory, but both require extremely basic conditions (pH ≥ 11) either for synthesis or for stability. It is unlikely that the ambient pH inside the organism, ranging from pH 5 in the silica deposition vesicle to pH 8 in the cytoplasm,[42,78] would be appropriate for the production or maintained solubility of these compounds. In lieu of such complexes, ordinary tetrafunctional organosilicates provide a simple model for the silicon starting material for biogenic silica synthesis in diatoms, and ab initio molecular orbital calculations show that formation of such compounds from alcohols, sugars, and multicarboxylic acids is thermodynamically favorable at intracellular conditions.[79−82]

Second, the mechanism of biogenic silica precipitation is still not fully understood, but it has been suggested that silica precipitation via amine catalysis occurs through predominantly electrostatic mechanisms whereby positively charged amine groups from polyamines interact to concentrate negatively charged silicate oligomers and foster their precipitation.[26,28,45,46] In diatoms, the local aggregation of silicate oligomers may be aided by phase-separation between a protein-containing phase and an aqueous silicate-containing phase.[27,30,83,84] These mechanisms provide an adequate model of silica precipitation when the starting material is silicic acid (obtained by prehydrolysis of an organosilicate) leading to rapid formation of silicate oligomers but do not address the possibility that silicic acid may not be the precursor to silica formation in vivo.

The proteins responsible for silica precipitation in vivo include the polylysine-containing silaffins in diatoms,[37,38] and the histidine-containing silicatein found in sponges.[40] On the basis of our findings, it would appear that organosilicate hydrolysis with amine catalysts does not occur through a single mechanism. Silica precipitation in diatoms occurs in the silica deposition vesicle at pH ≈ 5,[47,78] where the majority of amine groups found in polyamines and silaffins would exist in the protonated form. Furthermore, if polylysine and ethylamine, both with sp^3 nitrogen hybridization, are considered to behave similarly, then the lysines would bind in the more stable axially bound pentacoordinate structure, from which the energetic cost of proceeding through nucleophile-activated catalysis via a hexacoordinate structure is higher. The proton-transfer S_N2 mechanism would, therefore, be energetically favored.

The cellular machinery for precipitating silica in sea sponges is not as well characterized as that for diatoms, and the ambient pH of seawater, or an assumed neutral pH, would be reasonable estimates for the conditions under which sponges precipitate silica. It has been shown that isolated and purified silicatein, the histidine-containing protein isolated from sea sponges, can polymerize organosilicate hydrolysis and subsequent silica precipitation at pH 7 in vitro,[40] and that histidine at the catalytic site is required for precipitation.[39] Similarly, histidine-containing peptides from a phage display library have been demonstrated to precipitate silica at pH 7.5.[43] The pK_a of histidine in biological systems is estimated to be approximately 6.5,[85] indicating that the amine would exist predominantly in the conjugate base form. For imidazole, our calculated activation energies for nucleophile-assisted mechanism are lower than those for the proton-transfer mechanism. It is, therefore, entirely possible that organosilicate hydrolysis may occur through the nucleophile-activated substitution in organisms where histidine-containing proteins are found. These chemical mechanisms may act in cooperation with the physical mechanisms of silicate oligomer aggregation.[26,27,30,83,84]

Conclusions

We have attempted to elucidate the role of amines in chemical catalysis of organosilicate hydrolysis at circum-neutral pH values. Amines catalyze TMES hydrolysis by acting as proton-transfer agents that promote S_N2 hydrolysis. The same mechanism operates for organosilicates, such as TMOS, but the competing mechanism of nucleophile-activated substitution is also possible. Ultimately, the mechanism depends on the amine, the ambient pH, and on the nature of the starting silicon substrates.

Biogenic silica formation is mediated by proteins, where both physical and chemical interactions contribute to the catalytic ability of the protein. In this work, we have used small amine molecules to examine the *chemical* factors that may contribute to catalysis of organosilicate hydrolysis, which is the first step to silica formation. We have demonstrated that both the pH of the solution and the pK_a of protein amino acid side chains affect which pathway is used in hydrolysis. Thus, our study not only furthers our understanding of the potential chemcial mechanisms that certain biological systems may use to in silica formation

but it also provides information that may be useful for designing biomimetic pathways of sol−gel silica synthesis at circumneutral pH values.

Acknowledgment. We thank Prof. Robert West of the UW Department of Chemistry, and Dr. Charles Fry of the UW Chemistry Magnetic Resonance Facility for help with instrumentation and numerous helpful discussions. We are also grateful to Prof. Joel Pedersen for use of his ATR-FTIR spectrometer, and Prof. Robert Hamers and Jeremy Streifer for assistance in conducting XPS experiments. Finally, we thank Dr. Hieu Tran for assistance with computational modeling. Funding was provided by NSF EAR 020836 and Faculty "Startup Grants" to N. Sahai. NMR Spectrometer funding support: NSF CHE 9629688, NSF CHE 8813550, NIH 1 S10 RR04981-01.

Supporting Information Available: Final geometries in Cartesian coordinates of the stable penta- and hexacoordinate structures reported in this work and a graph of the Arrhenius plots for determination of the activation energy for TMES hydrolysis. This material is available free of charge via the Internet at http://pubs.acs.org.

References and Notes

(1) Iler, R. K. *The Chemistry of Silica*; John Wiley & Sons: New York, 1979.

(2) Brinker, C. J.; Scherer, G. W. *Sol−Gel Science. The Physics and Chemistry of Sol−Gel Processing*; Academic Press: Boston, MA, 1990.

(3) Kresge, C. T.; Leonowicz, M. E.; Roth, W. J.; Vartuli, J. C.; Beck, J. S. *Nature* **1992**, *359*, 710.

(4) Beck, J. S.; Vartuli, J. C.; Kennedy, G. J.; Kresge, C. T.; Roth, W. J.; Schrammt, S. E. *Chem. Mater.* **1994**, *6*, 1816.

(5) Pouxviel, J. C.; Boilot, J. P.; Beloeil, J. C.; Lallemand, J. Y. *J. Non-Cryst. Solids* **1987**, *89*, 345.

(6) Fyfe, C. A.; Aroca, P. P. *Chem. Mater.* **1995**, *7*, 1800.

(7) Rankin, S. E.; McCormick, A. V. *Magn. Reson. Chem.* **1999**, *37*, S27.

(8) Rankin, S. E.; Macosko, C. W.; McCormick, A. V. *J. Polym. Sci., Part A: Polym. Chem.* **1997**, *35*, 1293.

(9) Brinker, C. J.; Assink, R. A. *J. Non-Cryst. Solids* **1989**, *111*, 48.

(10) Brinker, C. J. *J. Non-Cryst. Solids* **1988**, *100*, 31.

(11) Kay, B. D.; Assink, R. A. *J. Non-Cryst. Solids* **1988**, *104*, 112.

(12) Alam, T. M.; Assink, R. A.; Loy, D. A. *Chem. Mater.* **1996**, *8*, 2366.

(13) Suda, S.; Iwaida, M.; Yamashita, K.; Umegaki, T. *J. Non-Cryst. Solids* **1996**, *197*, 65.

(14) Pouxviel, J. C.; Boilot, J. P. *J. Non-Cryst. Solids* **1987**, *94*, 374.

(15) Sanchez, J.; Rankin, S. E.; McCormick, A. V. *Ind. Eng. Chem. Res.* **1996**, *35*, 117.

(16) Rankin, S. E.; Sefcik, J.; McCormick, A. V. *J. Phys. Chem. A* **1999**, *103*, 4233.

(17) Tejedor-Tejedor, M. I.; Paredes, L.; Anderson, M. A. *Chem. Mater.* **1998**, *10*, 3410.

(18) Leyden, D. E.; Atwater, J. B. *J. Adhes. Sci. Technol.* **1991**, *5*, 815.

(19) Lippert, J. L.; Melpolder, S. B.; Kelts, L. M. *J. Non Cryst. Solids* **1988**, *104*, 139.

(20) Okumoto, S.; Fujita, N.; Yamabe, S. *J. Phys. Chem. A* **1998**, *102*, 3991.

(21) Kudo, T.; Gordon, M. S. *J. Phys. Chem. A* **2000**, *104*, 4058.

(22) Kudo, T.; Gordon, M. S. *J. Am. Chem. Soc.* **1998**, *120*, 11432.

(23) Damrauer, R.; Burggraf, L. W.; Davis, L. P.; Gordon, M. S. *J. Am. Chem. Soc.* **1988**, *110*, 6601.

(24) Burggraf, L. W.; Davis, L. P.; Gordon, M. S. In *Ultrastructure Processing of Advanced Ceramics*; Uhlmann, D. R., Ulrich, D. R., Eds.; John Wiley & Sons: New York, 1992; pp 47−55.

(25) Cypryk, M.; Apeloig, Y. *Organometallics.* **2002**, *21*, 2165.

(26) Belton, D. J.; Patwardhan, S. V.; Perry, C. C. *J. Mater. Chem.* **2005**, *15*, 4629.

(27) Belton, D.; Patwardhan, S. V.; Perry, C. C. *Chem. Commun.* **2005**, 3475.

(28) Belton, D.; Paine, G.; Patwardhan, S. V.; Perry, C. C. *J. Mater. Chem.* **2004**, *14*, 2231.

(29) Knecht, M. R.; Wright, D. W. *Langmuir* **2004**, *20*, 4728.

(30) Patwardhan, S. V.; Maheshwari, R.; Mukherjee, N.; Kiick, K. L.; Clarson, S. J. *Biomacromolecules* **2006**, *7*, 491.

(31) Patwardhan, S. V.; Mukherjee, N.; Steinitz-Kannan, M.; Clarson, S. J. *Chem. Commun.* **2003**, 1122.

(32) Patwardhan, S. V.; Clarson, S. J. *Silicon Chem.* **2002**, *1*, 207.

(33) Patwardhan, S. V.; Clarson, S. J. *Abstr. Pap. Am. Chem. Soc.* **2003**, *225*, U663.

(34) Roth, K. M.; Zhou, Y.; Yang, W. J.; Morse, D. E. *J. Am. Chem. Soc.* **2005**, *127*, 325.

(35) Delak, K. M.; Sahai, N. *Chem. Mater.* **2005**, *17*, 3221.

(36) Delak, K. M.; Sahai, N. *Chem. Mater.* **2005**, *17*, 4272.

(37) Poulsen, N.; Sumper, M.; Kroger, N. *Proc. Natl. Acad. Sci. U.S.A.* **2003**, *100*, 12075.

(38) Poulsen, N.; Kroger, N. *J. Biol. Chem.* **2004**, *279*, 42993.

(39) Zhou, Y.; Shimizu, K.; Cha, J. N.; Stucky, G. D.; Morse, D. E. *Angew. Chem., Int. Ed.* **1999**, *38*, 780.

(40) Cha, J. N.; Shimizu, K.; Zhou, Y.; Christiansen, S. C.; Chmelka, B. F.; Stucky, G. D.; Morse, D. E. *Proc. Natl. Acad. Sci. U.S.A.* **1999**, *96*, 361.

(41) Armbrust, E. V.; Berges, J. A.; Bowler, C.; Green, B. R.; Martinez, D.; Putnam, N. H.; Zhou, S. G.; Allen, A. E.; Apt, K. E.; Bechner, M.; Brzezinski, M. A.; Chaal, B. K.; Chiovitti, A.; Davis, A. K.; Demarest, M. S.; Detter, J. C.; Glavina, T.; Goodstein, D.; Hadi, M. Z.; Hellsten, U.; Hildebrand, M.; Jenkins, B. D.; Jurka, J.; Kapitonov, V. V.; Kroger, N.; Lau, W. W. Y.; Lane, T. W.; Larimer, F. W.; Lippmeier, J. C.; Lucas, S.; Medina, M.; Montsant, A.; Obornik, M.; Parker, M. S.; Palenik, B.; Pazour, G. J.; Richardson, P. M.; Rynearson, T. A.; Saito, M. A.; Schwartz, D. C.; Thamatrakoln, K.; Valentin, K.; Vardi, A.; Wilkerson, F. P.; Rokhsar, D. S. *Science* **2004**, *306*, 79.

(42) Hildebrand, M. *J. Nanosci. Nanotechnol.* **2005**, *5*, 146.

(43) Naik, R. R.; Brott, L. L.; Clarson, S. J.; Stone, M. O. *J. Nanosci. Nanotechnol.* **2002**, *2*, 95.

(44) Mizutani, T.; Nagase, H.; Fujiwara, N.; Ogoshi, H. *Bull. Chem. Soc. Jpn.* **1998**, *71*, 2017.

(45) Coradin, T.; Livage, J. *Colloids Surf., B* **2001**, *21*, 329.

(46) Coradin, T.; Durupthy, O.; Livage, J. *Langmuir* **2002**, *18*, 2331.

(47) Martin-Jezequel, V.; Hildebrand, M.; Brzezinski, M. A. *J. Phycol.* **2000**, *36*, 821.

(48) Corriu, R. J. P.; Leclercq, D.; Vioux, A.; Pauthe, M.; Phalippou, J. In *Ultrastructure Processing of Advanced Ceramics*; Mackenzie, J. D., Ulrich, D. R., Eds.; John Wiley & Sons: New York, 1988; pp 113−126.

(49) Chuit, C.; Corriu, R. J. P.; Reye, C.; Young, J. C. *Chem. Rev.* **1993**, *93*, 1371.

(50) Corriu, R. J. P.; Dabosi, G.; Martineau, M. *J. Organomet. Chem.* **1980**, *186*, 25.

(51) Corriu, R. J. P.; Dabosi, G.; Martineau, M. *J. Organomet. Chem.* **1978**, *154*, 33.

(52) Corriu, R. J. P.; Guerin, C.; Henner, B. J. L.; Wang, Q. *Organometallics* **1991**, *10*, 3200.

(53) Sahai, N., unpublished results, 2005.

(54) Hammond, G. S. *J. Am. Chem. Soc.* **1955**, *77*, 334.

(55) Voronkov, M. G.; Emelyanov, I. S.; Zelchan, G. I.; Dyakov, V. M.; Kuzentsov, I. G. *Khim. Geterotsik. Soedin.* **1975**, 35.

(56) Sidorkin, V. F.; Shagun, V. A.; Pestunovich, V. A. *Russ. Chem. Bull.* **1999**, *48*, 1049.

(57) Chernyshev, E. A.; Knyazev, S. P.; Kirin, V. N.; Vasilev, I. M.; Alekseev, N. V. *Russ. J. Gen. Chem.* **2004**, *74*, 58.

(58) Sorensen, O. W.; Ernst, R. W. *J. Magn. Reson.* **1983**, *51*, 477.

(59) Delak, K. M.; Farrar, T. C.; Sahai, N. *J. Non-Cryst. Solids* **2005**, *351*, 2244.

(60) Carr, H. Y.; Purcell, E. M. *Phys. Rev.* **1954**, *94*, 630.

(61) Meiboom, S.; Gill, D. *Rev. Sci. Instrum.* **1958**, *29*, 688.

(62) Vangeet, A. L. *Anal. Chem.* **1970**, *42*, 679.

(63) Frisch, M. J.; Trucks, G. W.; Schlegel, H. B.; Scuseria, G. E.; Robb, M. A.; Cheeseman, J. R.; Montgomery, J. A., Jr.; Vreven, T.; Kudin, K. N.; Burant, J. C.; Millam, J. M.; Iyengar, S. S.; Tomasi, J.; Barone, V.; Mennucci, B.; Cossi, M.; Scalmani, G.; Rega, N.; Petersson, G. A.; Nakatsuji, H.; Hada, M.; Ehara, M.; Toyota, K.; Fukuda, R.; Hasegawa, J.; Ishida, M.; Nakajima, T.; Honda, Y.; Kitao, O.; Nakai, H.; Klene, M.; Li, X.; Knox, J. E.; Hratchian, H. P.; Cross, J. B.; Bakken, V.; Adamo, C.; Jaramillo, J.; Gomperts, R.; Stratmann, R. E.; Yazyev, O.; Austin, A. J.; Cammi, R.; Pomelli, C.; Ochterski, J. W.; Ayala, P. Y.; Morokuma, K.; Voth, G. A.; Salvador, P.; Dannenberg, J. J.; Zakrzewski, V. G.; Dapprich, S.; Daniels, A. D.; Strain, M. C.; Farkas, O.; Malick, D. K.; Rabuck, A. D.; Raghavachari, K.; Foresman, J. B.; Ortiz, J. V.; Cui, Q.; Baboul, A. G.; Clifford, S.; Cioslowski, J.; Stefanov, B. B.; Liu, G.; Liashenko, A.; Piskorz, P.; Komaromi, I.; Martin, R. L.; Fox, D. J.; Keith, T.; Al-Laham, M. A.; Peng, C. Y.; Nanayakkara, A.; Challacombe, M.; Gill, P. M. W.; Johnson, B.; Chen, W.; Wong, M. W.; Gonzalez, C.; Pople, J. A. *Gaussian 03*, revision C.02; Gaussian, Inc.: Wallingford, CT, 2004.

(64) Lee, C. T.; Yang, W. T.; Parr, R. G. *Phys. Rev. B* **1988**, *37*, 785.

(65) Becke, A. D. *J. Chem. Phys.* **1993**, *98*, 5648.

(66) Hehre, W. J.; Radom, L.; Schleyer, P. v. R.; Pople, J. A. *Ab Intio Molecular Orbital Theory*; John Wiley & Sons: New York, 1986.

(67) Rablen, P. R.; Lockman, J. W.; Jorgensen, W. L. *J. Phys. Chem. A* **1998**, *102*, 3782.
(68) Felipe, M. A.; Xiao, Y.; Kubicki, J. D. In *Molecular Modeling Theory: Applications in the Geosciences*, Reviews in Mineralogy 42; Cygan, R. T., Kubicki, J. D., Eds.; Geochemical Society and Mineralogical Society of America: Washington, DC, 2001; pp 485−531.
(69) McQuarrie, D. A.; Simon, J. D. *Physical Chemistry: A Molecular Approach;* University Science Books: Sausalito, CA, 1997.
(70) Holmes, R. R. *Chem. Rev.* **1996**, *96*, 927.
(71) Aelion, R.; Loebel, A.; Eirich, F. *J. Am. Chem. Soc.* **1950**, *72*, 5705.
(72) Tandura, S. N.; Voronkov, M. G.; Alekseev, N. Y. *Curr. Top. Chem.* **1986**, *131*, 99.
(73) Bassindale, A. R.; Stout, T. *J. Chem. Soc. Chem. Commun.* **1984**, 1387.
(74) Schmidt, M. W.; Windus, T. L.; Gordon, M. S. *J. Am. Chem. Soc.* **1995**, *117*, 7480.
(75) Gordon, M. S.; Davis, L. P.; Burggraf, L. W. *Chem. Phys. Lett.* **1989**, *163*, 371.
(76) Lambert, J. B.; Lu, G., Singer, S. R.; Kolb, V. M. *J. Am. Chem. Soc.* **2004**, *126*, 9611.
(77) Asuncion, M. Z.; Hasegawa, I.; Kampf, J. W.; Laine, R. M. *J. Mater. Chem.* **2005**, *15*, 2114.
(78) Vrieling, E. G.; Gieskes, W. W. C.; Beelen, T. P. M. *J. Phycol.* **1999**, *35*, 548.
(79) Sahai, N.; Tossell, J. A. *Geochim. Cosmochim. Acta* **2001**, *65*, 2043.
(80) Sahai, N.; Tossell, J. A. *Inorg. Chem.* **2002**, *41*, 1993.
(81) Sahai, N. *Geochim. Cosmochim. Acta* **2004**, *68*, 227.
(82) Sahai, N. *Geochim. Cosmochim. Acta* **2005**, *69*, 5137.
(83) Sumper, M. *Science* **2002**, *295*, 2430.
(84) Brunner, E.; Lutz, K.; Sumper, M. *Phys. Chem. Chem. Phys.* **2004**, *6*, 854.
(85) Stryer, L. *Biochemistry*; W. H. Freeman and Company: New York, 1988.
(86) Schaftenaar, G.; Noordik, J. H. *J. Comput. Aided Mol. Des.* **2000**, *14*, 123.